A Fast Saturation Based Dehazing Framework with Accelerated Convolution and Attention Block

Shuocheng Wang, Jiaming Liu, Yilian Zhong, Ruoxi Zhu, Jiazheng Lian, Hao Zhang, Yibo Fan* State Key Laboratory of Integrated Chips and Systems, Fudan University

Abstract—Real-time image dehazing is crucial for applications such as autonomous driving, surveillance, and remote sensing, where haze can significantly reduce visibility. However, many deep learning algorithms are hindered by large model sizes. making real-time processing difficult to achieve. Several fast and lightweight dehazing networks rely on estimating K(x), but they often fail to deliver satisfying performance. In this paper, we present a novel fast dehazing framework built upon the saturation-based algorithm. We design a new convolution module called Feature Extraction Partial Convolution (FEPC), which is faster and achieves better performance than the vanilla 3×3 convolution. Additionally, we fully leverage the information redundancy between feature map channels by dividing it into two parts along the channel dimension and designing a Self-Cross Attention Block (SCAB). The reduction in channel count significantly reduces computational load and improves the framework's speed. Through extensive experiments, our method demonstrates not only a fast inference speed but also superior dehazing performance, providing a promising solution for real-time practical deployment. Our code will be available at https://github.com/superwsc/FSB-Dehazing-Framework.

Index Terms—Image Dehazing, Deep Learning, Saturation-Based, Speed

I. Introduction

In autonomous driving, clear visibility is essential for safety and accurate decision-making. However, haze may severely degrade the quality of images [1], [2], increasing the risk of navigation errors. While many dehazing algorithms can improve image clarity, real-time performance is critical to avoid delays that could lead to accidents. Therefore, it is necessary to develop a dehazing framework that not only delivers effective performance but also operates at a high speed to ensure the functioning of autonomous systems.

In the field of image dehazing, a classic Atmospheric Scattering Model (ASM [3]) was introduced to describe the formation of hazy images:

$$H(x) = J(x)t(x) + A(1 - t(x)), \tag{1}$$

where H(x) represents the hazy image, J(x) corresponds to the clean image, A denotes the atmospheric light, and t(x) represents the transmission map. Based on this model, many works estimate A and t(x) by leveraging specific priors and assumptions to restore the clean image. He *et al.* [4] introduced a straightforward dehazing method that uses the dark channel prior (DCP). Kim *et al.* [5] proposed a fast haze removal

This work was supported in part by the National Key R&D Program of China (2023YFB4502802), in part by the National Natural Science Foundation of China (62031009), in part by the "Ling Yan" Program for Tackling Key Problems in Zhejiang Province (No.2022C01098), in part by Alibaba Innovative Research (AIR) Program, in part by Alibaba Research Fellow (ARF) Program, in part by the Fudan-ZTE Joint Lab, in part by CCF-Alibaba Innovative Research Fund For Young Scholars.

Yibo Fan is the corresponding author.

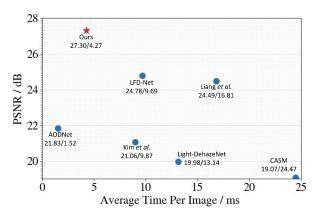


Fig. 1. Comparisons with other models. The PSNR/Time on HSTS-synthetic dataset of each model are labeled in the diagram.

algorithm that estimates medium transmission based solely on the scene radiance's saturation.

In recent years, many deep learning dehazing methods have been proposed. Some works such as PhysicsGAN [6] and RefineDNet [7] have large model sizes that hinder real-time performance. As for fast and lightweight dehazing algorithms, AODNet [8] combined A and t(x) into a single variable K(x) for direct estimation. Some subsequent K(x)-based works, such as Light-DehazeNet [9] and LFD-Net [10], also adopted this approach. However, directly estimating K(x) through a lightweight network is challenging and unlikely to yield satisfactory results because K(x) encompasses the two crucial variables of hazy image.

In this paper, we propose a fast saturation-based dehazing framework. Image saturation refers to the purity of colors in an image, which is more explainable and has a clearer physical meaning compared with K(x), thus it is easier for the network to estimate accurately. We also design a small and fast saturation estimation network which is integrated into our framework to improve the image quality. Our main contributions can be summarized as follows:

- We design a new dehazing framework built on saturationbased algorithm. By leveraging the interpretable characteristic of image saturation, we can estimate the clear image's saturation and calculate the transmission map more precisely, leading to improved dehazing performance and faster speed.
- We introduce a novel convolution module called Feature Extraction Partial Convolution (FEPC) and a new attention module called Self-Cross Attention Block (SCAB). Compared to traditional convolution and attention modules, FEPC and SCAB achieve both faster speed and

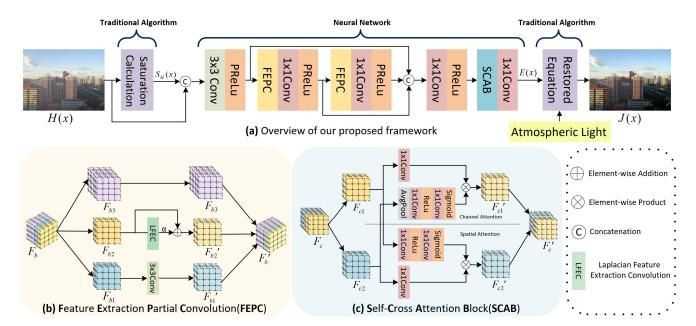


Fig. 2. (a) Overview of our proposed framework, which primarily consists of two traditional algorithm parts and one network part. The network part mainly comprises two FEPCs and one SCAB. (b) Structure of Feature Extraction Partial Convolution (FEPC). (c) Structure of Self-Cross Attention Block (SCAB).

superior performance.

 Comprehensive experiments on synthetic and real-world datasets show that our method delivers state-of-the-art (SOTA) image quality objectively and perceptually, while also achieving less processing time.

II. PROPOSED METHOD

A. The Saturation-based Dehazing Framework

Currently, many high-performance dehazing networks struggle to achieve real-time due to their large model sizes and computational complexity. Although there are some fast K(x)-based dehazing methods [8]–[10], they suffer from inaccurate K(x) estimation and poor image quality. As a result, we propose a saturation-based framework to achieve faster and more effective image dehazing. Its physical model, as described in [5], is shown below.

$$I_H(x) = (H^R(x) + H^G(x) + H^B(x))/3,$$
 (2)

$$S_H(x) = 1 - min(H^R(x), H^G(x), H^B(x))/I_H(x),$$
 (3)

$$t(x) = 1 - (I_H(x)/A) (1 - S_H(x)/S_J(x)), \qquad (4)$$

where $H^c(x)$ ($c \in \{R,G,B\}$) denotes the pixel value of RGB channels in the hazy image H(x), $I_H(x)$ represents the H(x)'s intensity, $S_H(x)$ is the saturation component of H(x) at location x, and $S_J(x)$ is the clean image J(x)'s saturation. For simplicity, we assume that the atmospheric light A is same in the entire image.

In Eq. (4), $S_J(x)$ needs to be estimated and [5] obtained an approximate condition of $S_J(x) \geq S_H(x)$, employing rough stretch functions such as $S_J(x) = S_H(x)(2 - S_H(x))$ to estimate $S_J(x)$. However, these functions fail to accurately capture the relationship between $S_J(x)$ and $S_H(x)$. Moreover, different regions in an image require different degrees of saturation stretching, making the use of a global stretch function inaccurate. Therefore, we propose a network to enhance

the accuracy and get a point-wise $S_J(x)$ estimation. Besides, multiplication and division in Eq. (4) can introduce extra computational overhead if we directly estimate $S_J(x)$. Integrating some of these calculations into the network estimation can help to reduce the latency without compromising accuracy. Eventually, our network directly estimates the following term:

$$E(x) = I_H(x) (1 - S_H(x)/S_J(x)). (5$$

By combining Eq. (1), Eq. (4) and Eq. (5), our final restored equation is obtained as,

$$J(x) = (H(x) - E(x)) / \left(1 - \frac{E(x)}{A}\right).$$
 (6)

Fig. 2(a) provides an overview of our framework. Firstly, the saturation of hazy image $S_H(x)$ is computed based on Eq. (2) and Eq. (3). $S_H(x)$ is then concatenated with the hazy image H(x) and they are used as the combined input to the network. The network estimates E(x) and our framework ultimately reconstructs the clean image J(x) through Eq. (6). The details of our network will be demonstrated in Section II-B.

B. Fast Saturation-Based Network

The neural network part in Fig. 2(a) is the primary bottleneck that impacts the computational speed of the entire framework. To address this issue, we propose a Feature Extraction Partial Convolution (FEPC) and a Self-Cross Attention Block (SCAB) to accelerate the network's speed.

1) Feature Extraction Partial Convolution: A large number of feature map channels can slow down convolution computation. Chen *et al.* [15] pointed out that the information across different channels often tends to be similar. Based on this observation, we only need to process a part of channels to decrease computational complexity and memory access. More specifically, we propose the Feature Extraction Partial Convolution (FEPC). FPEC can utilize fewer channels to more

TABLE I Comparisons between K(x)-based and Saturation-based using the same structure but different channel numbers.

	$Channels_{in}/Channels_{out}$			SOTS-outdoor		Inference on a 640×480 image				
Models	Conv1	Con2	Conv3	Conv4	Conv5	PSNR↑	<i>SSIM</i> ↑	Para(K)	MACs(G)	Time(ms)↓
K(x)-based [8]	3/3	3/3	6/3	6/3	12/1	22.7210	0.8965	1.761	0.5364	3.3030
Saturation-based	4/1	1/1	2/1	2/1	4/1	22.999	0.8801	0.202	0.0605	1.1081

TABLE II
QUANTITATIVE COMPARISONS WITH SOTA METHODS ON SOTS-OUTDOOR AND HSTS-SYNTHETIC DATASETS.

	SOTS-outdoor				HSTS-synthetic					
Models	PSNR ↑	SSIM↑	LPIPS↓	FID↓	Ave Time(ms)↓	PSNR↑	SSIM↑	LPIPS↓	FID↓	Ave Time(ms)↓
DCP [4]	17.1004	0.8496	0.1557	21.0140	36.751(CPU)	17.1943	0.8885	0.1335	35.7139	57.536(CPU)
Kim <i>et al</i> . [5]	21.9836	0.8641	0.1001	14.0828	9.667	21.0597	0.8703	0.0906	25.8773	8.974
DehazeNet [11]	22.8334	0.8886	0.0623	14.4877	1989.14(CPU)	23.9213	0.9061	0.0650	27.9113	1108.18(CPU)
AODNet [8]	22.7210	0.8965	0.0764	17.6676	1.5111	21.8300	0.9072	0.0711	35.6562	1.5183
Light-DehazeNet [9]	20.1538	0.8860	0.0867	29.2452	12.006	19.9842	0.8686	0.1058	72.7926	13.142
RefineDNet [7]	20.8112	0.8741	0.1106	18.6460	143.400	19.2457	0.7198	0.1266	39.3251	522.253
LFD-Net [10]	25.1263	0.9087	0.0524	14.7730	9.839	24.7813	0.8902	0.0677	33.0445	9.687
PSD [12]	15.0615	0.6974	0.1869	35.5434	334.622	14.6827	0.7346	0.1489	72.3399	273.371
PhysicsGAN [6]	20.3128	0.6458	0.1213	24.2499	7696.3	21.8449	0.8789	0.0924	54.2522	7594.9
Liang <i>et al.</i> [13]	24.1482	0.9139	0.0703	16.0549	17.037	24.4890	0.9003	0.0560	37.2933	16.812
CASM [14]	19.9379	0.8787	0.1299	24.4786	24.799	19.0735	0.8610	0.1177	52.9976	24.473
Ours	25.5383	0.9099	0.0613	11.8265	4.329	27.2990	0.9539	0.0286	11.647	4.272

The best and the second best results are highlighted in red and blue respectively.

swiftly extract the spatial information and high-frequency components from the feature map. It not only operates faster than conventional convolution but also delivers superior performance.

As illustrated in Fig. 2(b), we first split the feature map F_b along the channel dimension into three parts: F_{b1} , F_{b2} and F_{b3} . Then we pick F_{b1} with c_p channels to perform 3×3 convolution, resulting in F_{b1}' . Next, we select F_{b2} with another c_p channels for Laplacian Feature Extraction Convolution (LFEC) to extract high-frequency components. These components are then added to F_{b2} through a learnable coefficient α . This calculation results in F_{b2}' ,

$$F'_{b2} = F_{b2} + \alpha \times LFEC(F_{b2}).$$
 (7)

Due to Laplacian kernel's ability to efficiently capture high-frequency components, this operation effectively enhances the detailed information within the feature map. The F_{b3} with remaining $c-2c_p$ channels are copied directly to the corresponding positions in the output without any modification, which can effectively reduce the number of memory access and accelerate the computation. Finally, we concatenate $F_{b1}^{'}$, $F_{b2}^{'}$, and F_{b3} to obtain the final output $F_b^{'}$. It is important to note that F_{b3} is not redundant. This portion of information is valuable for the subsequent 1×1 convolution.

2) Self-Cross Attention Block: Many works have achieved impressive results using attention blocks [16], [17], but the large number of channels often significantly slows down the inference speed. Based on the similar idea described in Section II-B1, we find out that obtaining the attention map in an attention block does not require the involvement of all channels. By leveraging the similarity and diversity of information across different channels, we design the Self-Cross Attention Block (SCAB), where distinct attention mechanisms are applied within the feature map. Compared with the sequential stacking of multiple attention blocks, SCAB maintains superior performance while significantly reducing computational complexity and increasing processing speed.

As depicted in Fig. 2(c), the input feature map is evenly divided into two parts $(F_{c1} \text{ and } F_{c2})$ along the channel dimension. For F_{c1} , we apply channel attention using F_{c2} . F_{c2} is processed through global average pooling in the spatial domain, then passed through a series of convolutions and activation functions to generate a channel-wise attention map. This attention map is then multiplied with F_{c1} after it has been processed by a 1×1 convolution, resulting in F_{c1}' . The whole process can be described as follows,

$$F_{c1}^{'} = C_{1\times 1}(F_{c1}) \otimes \sigma(C_{1\times 1}(Relu(C_{1\times 1}(AvgPool(F_{c2}))))),$$
(8)

where \otimes represents element-wise product, σ represents sigmoid activation function and $C_{1\times 1}$ is a 1×1 convolution. For F_{c2} , we employ F_{c1} to generate a spatial attention map. The operation is similar as before and can be written in the following form,

$$F_{c2}^{'} = C_{1\times 1}(F_{c2}) \otimes \sigma(C_{1\times 1}(Relu(C_{1\times 1}(F_{c1})))). \tag{9}$$

The final output of SCAB is obtained by concatenating F'_{c1} and F'_{c2} together, resulting in F'_{c} .

III. EXPERIMENTS

A. Implementation Details

We train our model on the OTS dataset [18] using the Adam optimizer for 30 epochs, with a batch size of 12 and an initial learning rate of 0.01 on RTX 2080Ti GPU. The Charbonnier loss [19] is employed during training. The model's performance is evaluated on SOTS-outdoor and HSTS-synthetic datasets, as well as on real-world hazy images. In this paper, we set $c_p/c = 1/4$ in FEPC and the atmospheric light A = 0.9.

B. Comparisons of Estimation Method

Table I compares our saturation-based framework with the K(x)-based framework. Both of them employ the same network architecture used in [8], while the saturation-based uses significantly fewer channels. Despite their comparable dehazing performance, the saturation-based framework uses only 11.47% of parameters, and the processing time for a

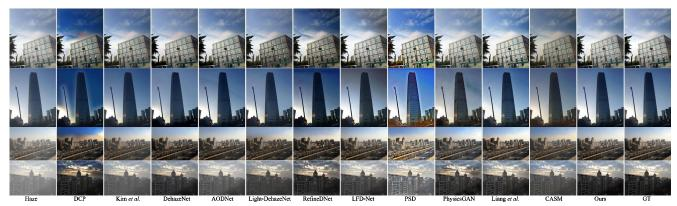


Fig. 3. Visual qualitative comparison on the synthetic datasets(zoom in for better visibility). The first two rows correspond to the SOTS-outdoor dataset, while the third row and fourth row correspond to the HSTS-synthetic dataset.



Fig. 4. Visual qualitative comparison on the real-world hazy images(zoom in for better visibility).

TABLE III

QUANTITATIVE COMPARISONS WITH SOTA METHODS ON REAL-WORLD
HAZY IMAGES.

Models	Para(K)/MACs(G)	Ave Time(ms)	$BRISQUE \downarrow$
DCP [4]	-/-	64.349(CPU)	27.3862
Kim <i>et al.</i> [5]	-/-	16.978	22.4119
DehazeNet [11]	8.3 / -	1775.45(CPU)	22.4603
AODNet [8]	1.761 / 0.6433	2.5021	22.9287
Light-DehazeNet [9]	30.187 / 11.083	21.195	22.8732
RefineDNet [7]	65795 / -	903.369	20.6436
LFD-Net [10]	90.239 / 32.8226	17.314	24.9008
PSD [12]	5316.3 / 1621.6	462.584	24.4038
PhysicsGAN [6]	11378.2 / 319.71	11822.4	20.0582
Liang <i>et al.</i> [13]	256.37 / 35.9052	26.1702	22.3164
CASM [14]	2.459 / 0.9272	38.095	23.5750
Ours	8.408 / 3.0493	6.6441	19.9654

The best and the second best results are highlighted in red and blue respectively.

 640×480 image is 33.55% compared to K(x)-based. This demonstrates the superior advantage of our saturation-based framework.

C. Comparisons of Dehazing Framework

We compare our method with 11 other SOTA methods. Table II showcases the superior performance of our approach on synthetic datasets, excelling in PSNR, SSIM [20], LPIPS [21] and FID [22] metrics, while also achieving impressive speed. Although AODNet [8] is faster than our method, our approach significantly outperforms it in terms of dehazing effectiveness. Fig. 3 indicates that DCP [4] and PSD [12] exhibit artifacts along the edges, while the results from Kim et al. [5], AODNet [8], DehazeNet [11] and Light-DehazeNet [9] have haze residuals (note the fourth row). The sky in the results of RefineDNet [7], LFD-Net [10], and CASM [14] appear darker with color distortion (note the first row). Our method can not only achieve fast processing speed but also better remove the haze in the image.

Fig. 4 and Table III present a comparison on real-world hazy images, demonstrating the superior BRISQUE [23] and speed advantage of our method. The results from Liang *et al.* [13], CASM [14], and PhysicsGAN [6] exhibit color distortion

and artifacts, alongside slower speed. Our results effectively preserve the original details of the image without any artifacts, making the images more realistic.

TABLE IV

RESULTS OF ABLATION STUDIES ON SOTS-OUTDOOR DATASET.

	PSNR ↑	SSIM↑	LPIPS↓	Time(ms)
FEPC \rightarrow 3×3 Conv	24.9250	0.9021	0.0521	5.523
w/o LFEC	24.8090	0.8976	0.0630	3.948
$SCAB \rightarrow CA + SA$	25.3140	0.9004	0.0625	4.937
w/o SCAB	24.2519	0.8842	0.0728	3.401
Ours	25 5383	0.9099	0.0613	4 329

The best and the second best results are highlighted in red and blue respectively.

D. Ablation Studies

Table IV details the impact of each component of our model. We replace FEPC with a common 3×3 convolution, and replace SCAB with a combination of channel attention and spatial attention. The results show that FEPC and SCAB can not only improve processing speed but also maintain high image quality. We also remove LFEC and observe the results. Although this result in a slight speed improvement, the network is unable to effectively capture the detailed information, leading to a significant decline in image quality. The framework is faster without SCAB but the performance is very poor because it can not effectively utilize the information in the feature map.

IV. CONCLUSION

In this paper, we present a fast saturation-based dehazing framework, offering real-time processing and outstanding dehazing performance. By incorporating Feature Extraction Partial Convolution and Self-Cross Attention Block, our framework not only optimizes inference speed but also improves image quality. Experimental results demonstrate that our saturation-based approach can maintain comparable dehazing quality as K(x)-based methods with fewer parameters and faster speed under same network structure. Our framework can deliver SOTA performance with notably faster speed than many existing deep learning models, underscoring its potential for practical dehazing applications.

REFERENCES

- [1] Yilian Zhong, Jiaming Liu, Xuan Huang, Jingjing Liu, Yibo Fan, and Minfeng Wu, "Cdcnet: A fast and lightweight dehazing network with color distortion correction," in *ICASSP 2024 2024 IEEE International Conference on Acoustics, Speech and Signal Processing (ICASSP)*, 2024, pp. 3020–3024.
- [2] Qi Zheng, Yibo Fan, Leilei Huang, Tianyu Zhu, Jiaming Liu, Zhijian Hao, Shuo Xing, Chia-Ju Chen, Xiongkuo Min, Alan C. Bovik, and Zhengzhong Tu, "Video quality assessment: A comprehensive survey," 2024.
- [3] Srinivasa G Narasimhan and Shree K Nayar, "Vision and the atmosphere," *International journal of computer vision*, vol. 48, pp. 233–254, 2002.
- [4] Kaiming He, Jian Sun, and Xiaoou Tang, "Single image haze removal using dark channel prior," *IEEE Transactions on Pattern Analysis and Machine Intelligence*, vol. 33, no. 12, pp. 2341–2353, 2011.
- [5] Se Eun Kim, Tae Hee Park, and Il Kyu Eom, "Fast single image dehazing using saturation based transmission map estimation," *IEEE Transactions* on *Image Processing*, vol. 29, pp. 1985–1998, 2020.
- [6] Jinshan Pan, Jiangxin Dong, Yang Liu, Jiawei Zhang, Jimmy Ren, Jinhui Tang, Yu-Wing Tai, and Ming-Hsuan Yang, "Physics-based generative adversarial models for image restoration and beyond," *IEEE Transactions on Pattern Analysis and Machine Intelligence*, vol. 43, no. 7, pp. 2449–2462, 2021.
- [7] Shiyu Zhao, Lin Zhang, Ying Shen, and Yicong Zhou, "Refinednet: A weakly supervised refinement framework for single image dehazing," *IEEE Transactions on Image Processing*, vol. 30, pp. 3391–3404, 2021.
- [8] Boyi Li, Xiulian Peng, Zhangyang Wang, Jizheng Xu, and Dan Feng, "Aod-net: All-in-one dehazing network," in 2017 IEEE International Conference on Computer Vision (ICCV), 2017, pp. 4780–4788.
- [9] Hayat Ullah, Khan Muhammad, Muhammad Irfan, Saeed Anwar, Muhammad Sajjad, Ali Shariq Imran, and Victor Hugo C. de Albuquerque, "Light-dehazenet: A novel lightweight cnn architecture for single image dehazing," *IEEE Transactions on Image Processing*, vol. 30, pp. 8968–8982, 2021.
- [10] Yizhu Jin, Jiaxing Chen, Feng Tian, and Kun Hu, "Lfd-net: Lightweight feature-interaction dehazing network for real-time remote sensing tasks," *IEEE Journal of Selected Topics in Applied Earth Observations and Remote Sensing*, vol. 16, pp. 9139–9153, 2023.
- [11] Bolun Cai, Xiangmin Xu, Kui Jia, Chunmei Qing, and Dacheng Tao, "Dehazenet: An end-to-end system for single image haze removal," *IEEE Transactions on Image Processing*, vol. 25, no. 11, pp. 5187–5198, 2016.
- [12] Zeyuan Chen, Yangchao Wang, Yang Yang, and Dong Liu, "Psd: Principled synthetic-to-real dehazing guided by physical priors," in Proceedings of the IEEE/CVF Conference on Computer Vision and Pattern Recognition (CVPR), June 2021, pp. 7180–7189.
- [13] Yudong Liang, Bin Wang, Wangmeng Zuo, Jiaying Liu, and Wenqi Ren, "Self-supervised learning and adaptation for single image dehazing," 07 2022, pp. 1112–1118.
- [14] Xudong Wang, Xi'ai Chen, Weihong Ren, Zhi Han, Huijie Fan, Yandong Tang, and Lianqing Liu, "Compensation atmospheric scattering model and two-branch network for single image dehazing," *IEEE Transactions on Emerging Topics in Computational Intelligence*, vol. 8, no. 4, pp. 2880–2896, 2024.
- [15] Jierun Chen, Shiu-hong Kao, Hao He, Weipeng Zhuo, Song Wen, Chul-Ho Lee, and S.-H. Gary Chan, "Run, don't walk: Chasing higher flops for faster neural networks," in 2023 IEEE/CVF Conference on Computer Vision and Pattern Recognition (CVPR), 2023, pp. 12021–12031.
- [16] Jie Hu, Li Shen, and Gang Sun, "Squeeze-and-excitation networks," in Proceedings of the IEEE Conference on Computer Vision and Pattern Recognition (CVPR), June 2018.
- [17] Sanghyun Woo, Jongchan Park, Joon-Young Lee, and In So Kweon, "Cbam: Convolutional block attention module," in *Proceedings of the European Conference on Computer Vision (ECCV)*, September 2018.
- [18] Boyi Li, Wenqi Ren, Dengpan Fu, Dacheng Tao, Dan Feng, Wenjun Zeng, and Zhangyang Wang, "Benchmarking single-image dehazing and beyond," *IEEE Transactions on Image Processing*, vol. 28, no. 1, pp. 492–505, 2019.
- [19] P. Charbonnier, L. Blanc-Feraud, G. Aubert, and M. Barlaud, "Two deterministic half-quadratic regularization algorithms for computed imaging," in *Proceedings of 1st International Conference on Image Processing*, 1994, vol. 2, pp. 168–172 vol.2.

- [20] Zhou Wang, A.C. Bovik, H.R. Sheikh, and E.P. Simoncelli, "Image quality assessment: from error visibility to structural similarity," *IEEE Transactions on Image Processing*, vol. 13, no. 4, pp. 600–612, 2004.
- [21] Richard Zhang, Phillip Isola, Alexei A. Efros, Eli Shechtman, and Oliver Wang, "The unreasonable effectiveness of deep features as a perceptual metric," in 2018 IEEE/CVF Conference on Computer Vision and Pattern Recognition, 2018, pp. 586–595.
- [22] Ali Borji, "Pros and cons of gan evaluation measures," *Computer Vision and Image Understanding*, vol. 179, pp. 41–65, 2019.
- [23] Anish Mittal, Anush Krishna Moorthy, and Alan Conrad Bovik, "Noreference image quality assessment in the spatial domain," *IEEE Transactions on Image Processing*, vol. 21, no. 12, pp. 4695–4708, 2012.